Tensile, Low Cycle Fatigue, and Very High Cycle Fatigue Characterizations of Advanced Single Crystal Nickel-Based Superalloys

Luciana Maria Bortoluci Ormastroni, Satoshi Utada, Jérémy Rame, Lorena Mataveli Suave, Kyoko Kawagishi, Hiroshi Harada, Patrick Villechaise, and Jonathan Cormier

Abstract

Tensile and fatigue life variabilities are investigated for new-generation single crystal Ni-based superalloys: the 3rd generation CMSX-4 Plus, the 6th generation TMS-238, and a newer Ni-based superalloy, TROPEA containing Pt. Consistently from the results of previous research, very high cycle fatigue (VHCF) properties at the chosen condition of T = 1000 °C/$R_\varepsilon = -1/f$ = 20 kHz are mainly influenced by the solidification/homogenization pore size and position. TROPEA alloy has the best low cycle fatigue (LCF) life among all tested alloys at 650 °C and $R_\sigma = 0.05/f$ = 0.5 Hz. To better understand the influence of chemical composition on the LCF endurance, tensile properties were investigated using nine different single crystalline alloys at 650 °C with the strain rate of 5×10^{-4} s^{-1}. The yield stress is directly affected by the chemical composition of the Ni-based superalloys, and alloys with high contents of Ti and Ta have a higher yield stress, due to an increased shearing resistance of γ' precipitates. Hence, the yield stress is the main control parameter of LCF at the selected condition. No influence of chemical composition on VHCF life durability has been observed, in good agreement with previous studies.

Keywords

Ni-based superalloys • Single crystal • Low cycle fatigue • Very high cycle fatigue • Tensile properties

Introduction

With a global increase in air traffic, a growth of 7.4 pct. in 2018 and another 5 pct. projected growth in 2019 [1], cleaner in terms of NO_x, CO, and CO_2 emissions, and cost-effective aero-engines, in terms of fuel consumption, are required. Advanced single crystal (SX) Ni-based superalloys are necessary to achieve higher operating temperatures, especially in the first stage blades and vanes, in addition to more efficient internal cooling systems and advanced thermal barrier coatings [2–4]. Since fatigue is responsible for most of the crack initiation events and failure for internally cooled blades [5], the present study is especially focusing on the fatigue life durability of three recently developed SX Ni-based superalloys: the 3rd generation CMSX-4 Plus [6], the 6th generation TMS-238 [7], and TROPEA [8, 9].

CMSX-4 Plus has been chosen in this study as a reference alloy, given the fact that currently most advanced aero-engine blades are manufactured with 3rd generation SXs or eventually with 4th generation having very good creep properties [6, 10, 11]. TMS-238, a 6th generation that probably presents the best compromise between (very) high-temperature creep properties and oxidation resistance, has been chosen since very few fatigue data exist for this alloy [7]. TROPEA is a new-generation Pt-containing superalloy which has recently been developed between ISAE-ENSMA/Institut Pprime and SAFRAN in France. It is considered as a potential alloy for future airfoils [8, 9]. The unique features of this alloy are a very high Ta content to increase the resistance to γ' shearing, a reduced Re content to preserve density and cost, and an addition of 1.95 wt. pct. Pt. The main idea behind the development of this alloy was to have a good environmental

L. M. Bortoluci Ormastroni (✉) · S. Utada · P. Villechaise · J. Cormier
Physics and Mechanics of Materials Department, Institut Pprime, UPR CNRS 3346, ISAE-ENSMA, 1 avenue Clément Ader, BP 40109, 86961 Futuroscope-Chasseneuil Cedex, France
e-mail: luciana-maria.bortoluci-ormastroni@ensma.fr

S. Utada · J. Rame
SAFRAN Aircraft Engines, Site de Villaroche, Rond-Point René Ravaud - Réau, 77550 Moissy-Cramayel, France

L. Mataveli Suave
SAFRAN Tech, PFX, 171 Boulevard Valmy, 92700 Colombes, France

K. Kawagishi · H. Harada
National Institute for Materials Science (NIMS), 1-2-1 Sengen, Tsukuba, Ibaraki 305-0047, Japan

S. Tin et al. (eds.), *Superalloys 2020*, The Minerals, Metals & Materials Series,
https://doi.org/10.1007/978-3-030-51834-9_33

resistance, to have a low γ/γ' lattice misfit by increasing the γ' lattice parameter, and to maximize the strength and the stability of the γ' phase above 1200 °C by forming a (Ni, Pt)$_3$ (Al, Ti, Ta) $L1_2$ structure [5, 8, 12, 13].

Pt is a very effective solid solution strengthener as a substrate element [14], and it is aimed to reduce the complexity of Ni-based superalloy coating process eliminating a bond coating step as the superalloy itself presents high environmental resistance [15, 16]. It is known that the Pt is not as much effective as Ta or Mo to strength the material at temperatures under 650 °C [17, 18]. However, the influence of the Pt element on the tensile and fatigue properties in SX Ni-based superalloys is not well understood.

For the fatigue properties evaluations, very high cycle fatigue (VHCF) at T = 1000 °C/$R_\varepsilon = -1/f$ = 20 kHz and low cycle fatigue (LCF) at T = 650 °C/R_σ = 0.05/f = 0.5 Hz were chosen to simulate service conditions of the profile and the blade root, respectively. In addition to tensile tests at 650 °C for the three targeted alloys, other tests were performed using MAR-M200 + Hf, AM1, AM3, René N4, MC2, René N5, PWA 1484, René N6, and MCNG to analyze the influence of chemical compositions on yield stress (YS). The aim of these additional tests will be to better understand the role of chemistry on the fatigue durability at low temperature of the three alloys mainly studied in this article. Finally, it has to be noted that HCF/VHCF durability is a certifying criterion of airfoils according to airworthiness authorities (e.g., EASA and FAA) [19–22].

Material and Experimental Techniques

SX Ni-Based Superalloys Chemical Composition

SX bars of CMSX-4 Plus and TROPEA were prepared at SAFRAN Tech PFX in Gennevilliers, France, while TMS-238 bars were prepared at National Institute for Materials Science (NIMS), Japan. The bars were solidified with a 14-mm diameter and the longitudinal direction close to [001]. The misorientation from the perfect [001] orientation is less than 13°. CMSX-4 Plus and TROPEA were solutioned and aged at Institut Pprime, and TMS-238 was solutioned and aged at NIMS.

To better understand the influence of chemical composition on YS at 650 °C, the authors chose nine different SX Ni-based superalloys. The bars have been solidified with nearly the same solidification parameters. Misorientation of the bars was less than 5° from [001]. These alloys are fully heat-treated to optimize the microstructure.

The chemical compositions in wt. pct. of the investigated alloys are presented in Table 1. The heat treatment (HT) conditions of TROPEA, CMSX-4 Plus, and TMS-238 are described in Table 2.

Mechanical Tests

Two different fatigue conditions were investigated, all performed with a sinusoidal waveform. The fatigue testing conditions were chosen to cover different temperature/stress states encountered in high-pressure turbine blades. Strain-controlled VHCF tests were performed at 1000 °C, $f = 20 \pm 0.5$ kHz, $R_\varepsilon = -1$ with an ultrasonic fatigue machine used in previous studies [11]. The specificities and details of the machine and the specimen geometry are detailed in the literature [19, 21]. Load-controlled LCF tests were conducted using an electro-mechanic Instron 8562 machine at 650 °C, f = 0.5 Hz, R_σ = 0.05. Specimens used for these tests have a 13 mm gauge length, a ~4.3 mm gauge diameter, and a 56 mm total length.

All specimens tested in fatigue were low-stress polished up to a mirror finish with 1 µm diamond paste to remove residual stresses introduced by the machining process and remaining scratches.

Tensile tests were performed using an electro-mechanical Instron 8562 machine at 650 °C. Strain measurements were ensured with an extensometer, equipped with ceramics arms, positioned onto the gauge section of the specimens. The tensile tests were performed using a strain rate of 5×10^{-4} s^{-1}. Cylindrical specimens having a 14 mm gauge length, a 4 mm gauge diameter, and a total length of 42 mm were used. Low-stress mechanical polishing up to a 4000 grade SiC paper was performed on the cylindrical specimens to remove remaining scratches and the plastically deformed layer before tensile tests. The polishing procedure avoids recrystallization during high-temperature monotonic tests.

Microstructural Characterizations

A combination of optical and scanning electron microscopy (OM and SEM, respectively) observations was used to characterize the microstructure of each alloy. The pore size distribution and the area fraction were determined by OM using unetched mirror-polished specimens, up to a 1-µm diamond paste polishing grade, sliced from heat-treated bars. Metallographic observations were performed roughly on (001) plane, i.e., perpendicular to the solidification direction.

The γ' size was determined from scanning electron microscope (SEM) observations using JEOL JSM-7000F field emission gun microscope operating at 25 kV, at a working distance of ~10 mm. For such SEM observations, specimens were previously polished up to a mirror finish and were etched for 8 to 10 s using aqua regia (1/3 HNO_3 + 2/3 HCl, vol. parts) at ~4 °C. Pore size, γ' size distribution, and γ/γ' eutectics area fraction were determined by image analyses using ImageJ software and specifically developed algorithms [23, 24].

Table 1 Nominal chemical composition of SX Ni-based superalloys examined (in wt. pct.)

Alloy	Ni	Cr	Mo	Co	W	Re	Al	Ti	Ta	Pt	Ru	Hf	C	B	Nb	Zr
TROPEA	Bal.	6.5	0.6	9.0	6.0	1.0	5.6	1.0	9.0	2.0	/	0.1	/	/	/	/
CMSX-4 Plus	Bal.	3.5	0.6	10	6.0	4.8	5.7	0.85	8.0	/	/	0.1	/	/	/	/
TMS-238	Bal.	4.6	1.1	6.5	4.0	6.4	5.9	/	7.6	/	5.0	0.1	/	/	/	/
MAR-M200 +Hf	Bal.	9.0	/	10.0	12.5	/	5.0	2.0	/	/	/	1.6	0.15	0.015	1.0	0.05
AM1	Bal.	7.8	2.0	6.5	5.7	/	5.2	1.1	7.9	/	/	0.05	/	/	/	/
AM3	Bal.	8.0	2.2	5.5	5.0	/	6.0	2.0	3.5	/	/	/	0.15	/	/	/
René N4	Bal.	9.8	1.5	7.4	5.9	/	4.2	3.5	4.7	/	/	0.1	0.06	0.004	0.5	/
MC2	Bal.	8.0	2.0	5.0	8.0	/	5.0	1.5	6.0	/	/	/	/	/	/	/
René N5	Bal.	7.0	2.0	8.0	5.0	3.0	6.2	/	7.0	/	/	0.15	0.05	/	0.2	/
PWA 1484	Bal.	4.9	2.0	9.8	5.9	3.0	5.7	0.02	8.6	/	/	0.1	/	/	/	/
René N6	Bal.	4.0	1.0	11.7	6.0	5.23	5.7	0.04	6.9	/	/	0.2	/	/	/	/
MCNG	Bal.	4.0	1.0	/	5.0	4.0	6.0	0.5	5.0	/	4.0	0.1	/	/	/	/

Table 2 Heat treatment conditions for TROPEA, CMSX-4 Plus, and TMS-238

Alloy	TROPEA	CMSX-4 PLUS	TMS-238
Solution heat treatment	1300 °C/24 h/AQ (heating rate 2 °C/min from 1200 °C)	1340 °C/15 h/AQ (heating rate 2 °C/min from 1200 °C)	1300 °C/1 h +1310 °C/1 h + 1335 °C/3 h + 1345 °C/20 h/AQ
AGING 1	1200 °C/1 h/AQ	1163 °C/3 h/AQ	1150 °C/2 h/AQ
AGING 2	870 °C/16 h/AQ	1100 °C/4 h/AQ	870 °C/20 h/AQ
AGING 3	/	870 °C/20 h/AQ	/

After the mechanical testing, fractographic observations were performed using JEOL JSM-7000F SEM, using the secondary (SEI) and backscattered (BSE) electron imaging modes. Investigation of the γ/γ' microstructure evolution after fatigue tests was also performed in longitudinal cross section, with the same polishing procedures and equipment described above.

Results

Metallurgical Defect Characterization

The microstructural characterization parameters are summarized in Table 3. Given the narrow solution window of TROPEA [9], specimens were left with a 10–13% remaining eutectics fraction. All of the superalloys present a similar pore area fraction of 1.3–1.6% and a maximum pore diameter between 80 and 120 µm.

The γ/γ' microstructures in primary dendrite arms after full HTs are presented in Fig. 1. A regular γ/γ' cuboidal microstructure is obtained. The results for CMSX-4 Plus and TROPEA show a comparable value of γ'-precipitate average edge length around 500 nm and a γ channel width around 60–70 nm. TMS-238 presents a γ'-precipitate average edge length around 235 nm and a γ channel width around 50 nm.

Very High Cycle Fatigue at 1000 °C

The S-N diagram gathering all VHCF results obtained at 1000 °C is presented in Fig. 2a. Results of CMSX-4 Plus with the HT described in Table 2, CMSX-4 Plus with a standard homogenization (STD), and CMSX-4 from a previous study [11] are inserted in the same figure. Their maximum pore size is ~100 µm [11].

At high stresses, TMS-238 presented a VHCF lifetime one order of magnitude higher than the lifetime presented by TROPEA and CMSX-4 Plus. As already documented by Cervellon et al. [20], for $R = -1$ and a limit of 10^9 cycles, the crack initiation always starts from casting pores. Similar results have also been obtained in the present study for all three main alloys, as illustrated in Fig. 2b, c. The rough region present around the crack initiating casting pore is a characteristic of VHCF crack initiation mechanism [20, 22].

Low Cycle Fatigue at 650 °C

The S-N diagram at 650 °C/$R_\sigma = 0.05$ and $f = 0.5$ Hz is presented in Fig. 3a. Results obtained from a previous study of Bortoluci et al. [11] have been added in this plot using CMSX-4 Plus specimens in the same testing conditions and machine. CMSX-4 Plus and TROPEA have a comparable

Table 3 Stereological characterizations of SX Ni-based superalloys examined

	γ'-Precipitate average edge length (nm)		γ Channel width (nm)	Pore's area fraction (Pct.)	Pore's maximum diameter (μm)	Eutectic's area fraction (Pct.)
	Primary dendrite arm	Interdendritic region				
TROPEA	471 ± 91	482 ± 71	71 ± 15	1.5	120	10 - 13
CMSX-4 – Plus	525 ± 91	533 ± 157	60 ± 12	1.3	100	0
TMS-238	234 ± 24	293 ± 53	43 ± 8	1.6	80	0
MAR-M200 +Hf	405 ± 81	/	81 ± 25			
AM1	465 ± 62	360 ± 52	52 ± 19			
AM3	440 ± 113	/	60 ± 20			
René N4	418 ± 91	440 ± 88	98 ± 42			
MC2	415 ± 77	477 ± 18	67 ± 17			
René N5	288 ± 31	369 ± 26	13 ± 7			
PWA 1484	316 ± 46	404 ± 64	46 ± 16			
René N6	380 ± 75	384 ± 46	54 ± 16			
MCNG	375 ± 70	349 ± 69	64 ± 20			

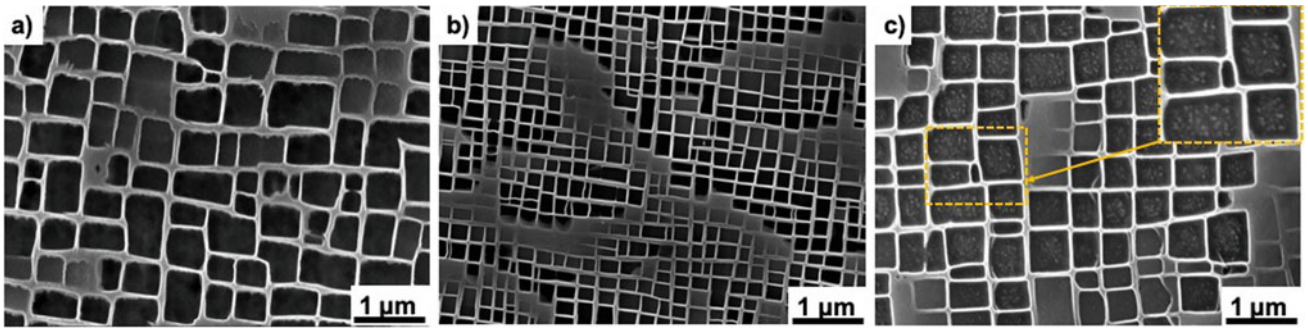

Fig. 1 γ/γ' microstructure along a (001) plane before mechanical testing. The images were taken inside the primary dendrite arm in CMSX-4 Plus (**a**), TMS-238 (**b**), and TROPEA (**c**). Detail of the γ-like particles within γ' precipitates in TROPEA specimens is shown as the insert in (**c**)

LCF durability within the σ_{max} range of 930–1000 MPa. TMS-238 has lower lifetime variability.

Under these LCF fatigue conditions, crack initiation occurred at casting pores, Fig. 3b, c. This observation is in good agreement with previous LCF results from Steuer et al. using AM1 under similar conditions [25]. Neither γ'-precipitate rafting nor recrystallization layer was identified in the internal microstructure of specimens after failure.

Tensile Tests

The main objective of tensile tests at 650 °C is to interpret the LCF behaviors as the maximum applied stress is approaching YS.

Tensile curves are presented in Fig. 4, and corresponding YS defined at 0.2 and 0.05 pct. of plastic offsets, ultimate tensile stress, strain at failure, and a partition coefficient is presented in Table 4.

The targeted superalloys have a specific yielding behavior at this condition. TROPEA shows a higher YS of 1027 MPa and a higher ultimate tensile stress compared to CMSX-4 Plus. Nevertheless, both of them exhibit a good elongation which is a typical tensile behavior in SX Ni-based superalloys at this temperature and strain rate [26, 27]. TMS-238 presents a particular tensile behavior with lower YS of 883 MPa. However, this superalloy shows a spectacular hardening, leading to an ultimate tensile stress equivalent to the ones observed for CMSX-4 Plus and TROPEA alloys.

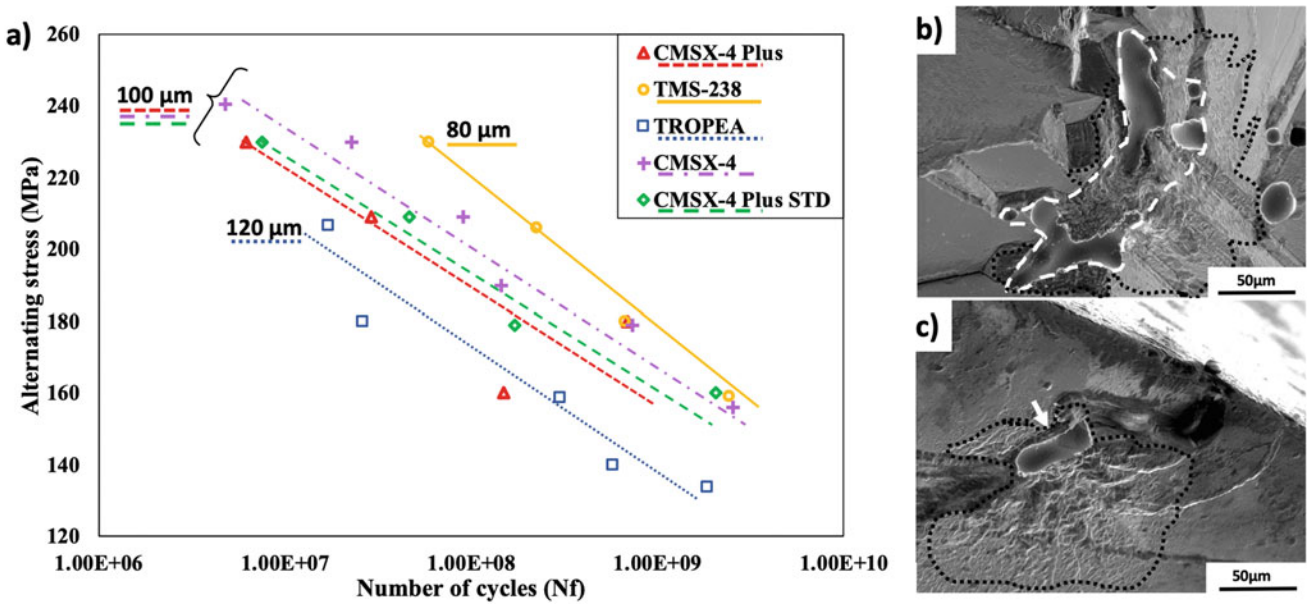

Fig. 2 S-N diagram at 1000 °C, $R_\varepsilon = -1/f = 20$ kHz. The alternating stress σ_a is plotted as a function of the number of cycles to failure (**a**), the corresponding maximum pore diameters (micrometer) are shown in black. Typical crack initiation sites in TMS-238 (**b**), and TROPEA (**c**) specimens after failure at $\sigma_a = 180$ MPa. Pores serving as main crack initiation sites have been highlighted using white dotted curves and white arrow, respectively. The black dotted curves highlight the rough region. CMSX-4 Plus, CMSX-4 Plus STD, and CMSX-4 data are extracted from the literature [11, 20]

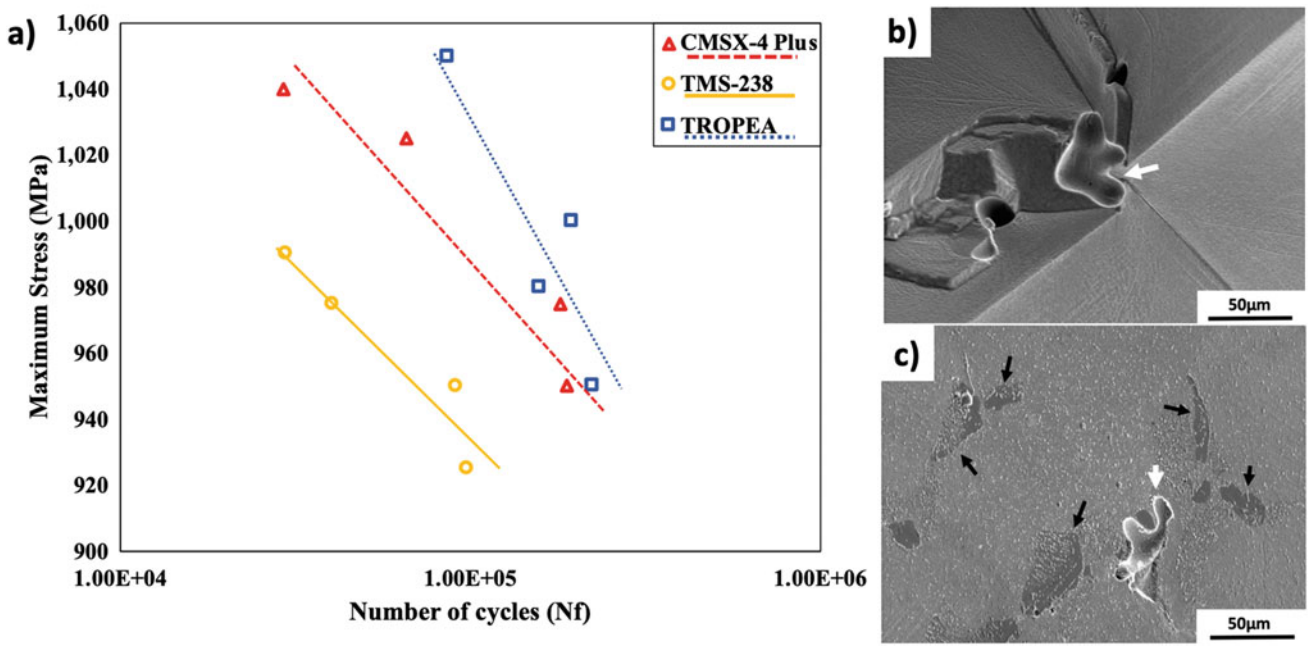

Fig. 3 S-N diagram at 650 °C, $R_\sigma = 0.05/f = 0.5$ Hz. The maximum stress σ_{max} is plotted as a function of the number of cycles to failure. Typical crack initiation sites after LCF tests at $\sigma_{max} = 950$ MPa. Crack initiation from an internal pore for TMS-238 (**b**) and from an internal pore connected to a γ/γ' eutectic for TROPEA (**c**). The white arrows highlight the casting/homogenization pores. The black arrows in (**c**) highlight the presence of eutectics. CMSX-4 Plus data are extracted from the literature [11]

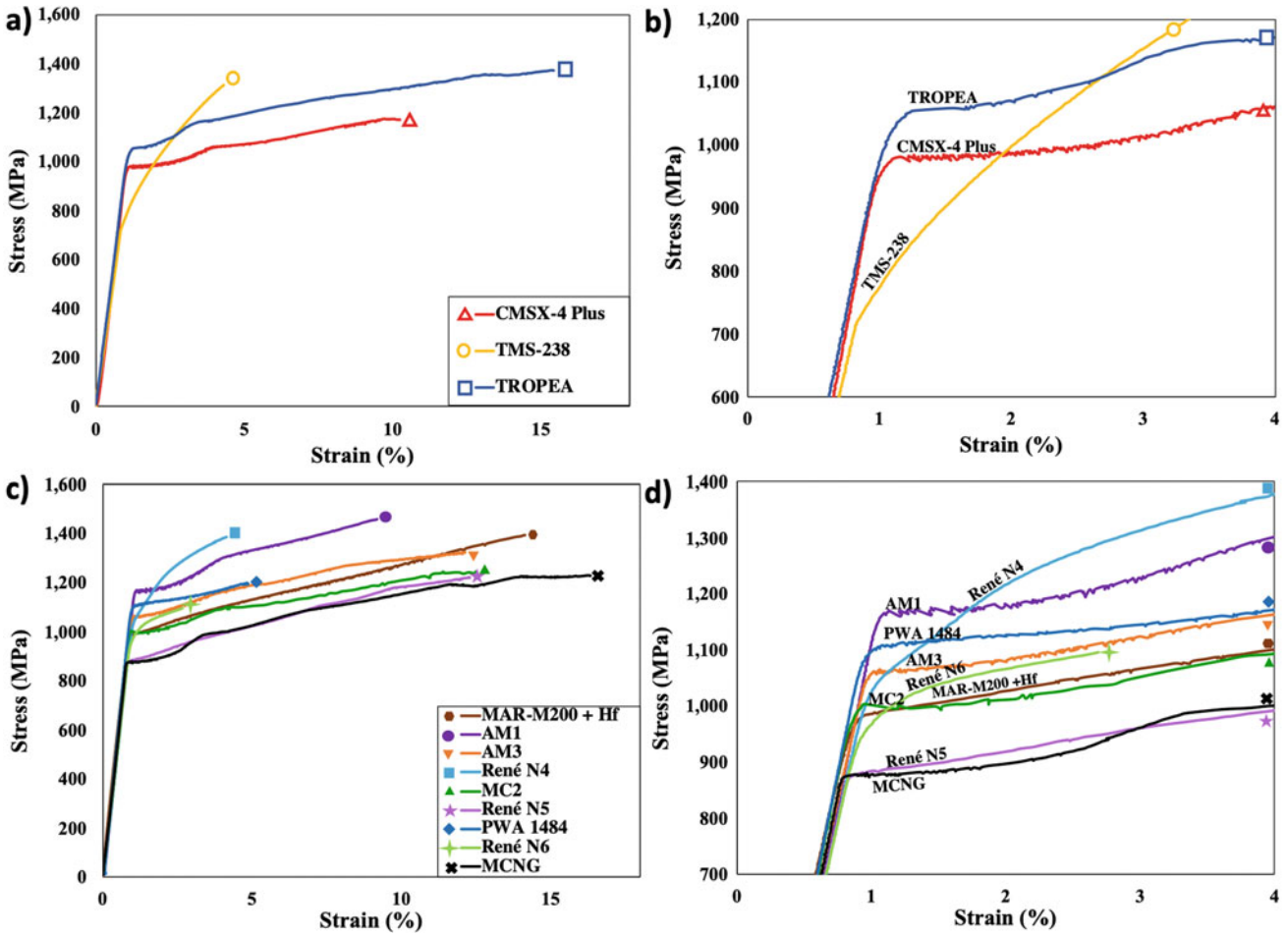

Fig. 4 Tensile curves representing the true stress versus true strain at 650 °C/5.0 × 10^{-4} s^{-1} for CMSX-4 Plus [11], TMS-238, and TROPEA (**a**) and a magnified plot around the YS (**b**). The nine additional SX Ni-based superalloys investigated (**c**) and a magnified plot around the YS (**d**)

Table 4 Tensile properties at 650 °C/5 × 10^{-4} s^{-1} of SX Ni-based superalloys examined

Superalloy	Yield stress 0.2 pct. of plastic offset (MPa)	Yield stress 0.05 pct. of plastic offset (MPa)	Ultimate tensile stress (MPa)	Strain at failure (Pct.)	$\frac{X_{Ti}+X_{Ta}}{X_{Al}}$[a]
TROPEA	1058	1047	1370	13.5	0.37
CMSX-4 Plus [11]	979	965	1160	8.5	0.30
TMS-238	883	736	1310	3.0	0.19
MAR-M200 +Hf	991	981	1400	12.0	0.25
AM1	1164	1162	1460	7.5	0.35
AM3	1058	1056	1320	10.0	0.29
René N4	1074	1024	1385	2.5	0.67
MC2	1000	975	1240	10.5	0.17
René N5	882	876	1220	10.0	0.17
PWA 1484	1106	1089	1200	3.5	0.23
René N6	1006	947	1095	1.5	0.19
MCNG	876	874	1230	15.0	0.36

[a]X concentration in atomic percent

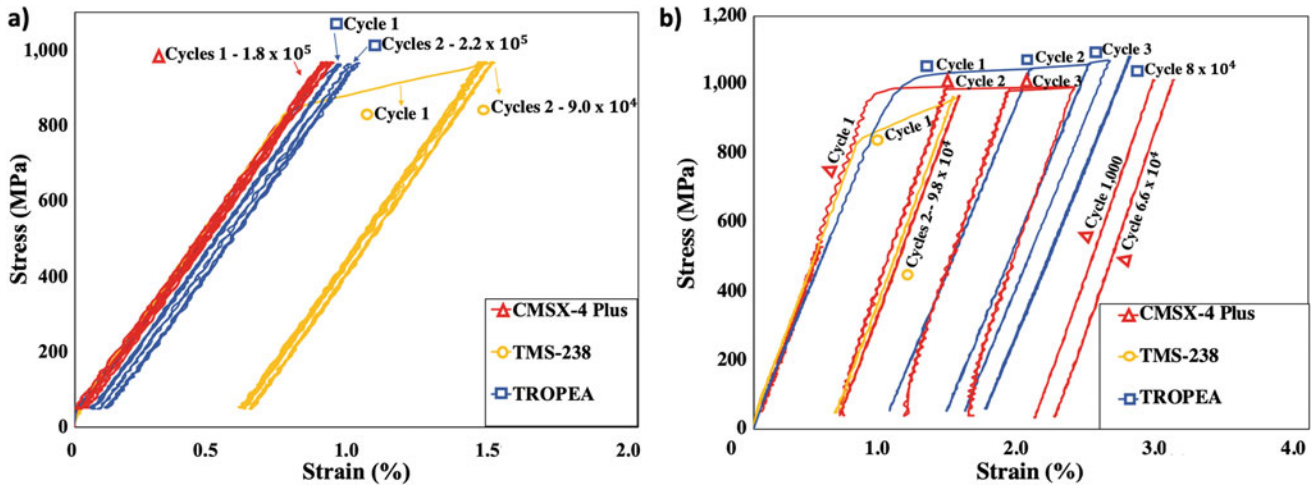

Fig. 5 True stress (MPa) versus true strain (%) diagram at 650 °C, R_σ = 0.05/f = 0.5 Hz/σ_{Max} = 950 MPa (**a**). True stress (MPa) versus true strain diagram at 650 °C, R_σ = 0.05/f = 0.5 Hz Normalized (σMax/YS) = 1.05 (**b**). The cycles and the specimens lifetime are labeled in the figure. CMSX-4 Plus data are extracted from the literature [11]

Note that these specific tensile behaviors have been observed in several specimens machined out from different bars with different orientations close to the [001] crystallographic orientation.

Discussion

A special attention will then be paid to the relation between chemistry and the mechanical properties of the superalloys in the following discussion.

Performance of TMS-238, CMSX-4 Plus, and TROPEA in VHCF

As already documented by Bortoluci et al. [11], and more specifically investigated by Cervellon et al. [20], the effect of pore size is much stronger than the presence of other metallurgical defects in the VHCF domain under fully reversed conditions. Hence, the durability of the investigated superalloys under VHCF conditions at R_ε = −1/1000 °C is mainly dependent on the pore size and position with respect to the surface, as described in Table 3.

From Fig. 2a, TMS-238 presents a superior lifetime, mainly at very high stresses. Moreover, pores in TMS-238 are 20% smaller than CMSX-4 Plus and 40% smaller than TROPEA. These differences in pore size probably result from minor variations in withdrawal rates/thermal gradients during the solidification process and/or casting mold thickness since SX bars had the same diameter. From past investigations [11, 20], the solidification parameters are the most important criteria controlling the VHCF lifetime variability. In fact, comparing the results obtained in this project with all the database of Institut Pprime for the same VHCF conditions [19], the TMS-238 performance is higher, almost reaching the lifetime of AM1/MCNG HIPed specimens [11, 19].

The chemical composition of the superalloys seems to have no impact on the VHCF lifetime variability under fully reversed conditions, in good agreement with our previous results [20]. A contribution of the chemistry of the alloys to the VHCF lifetime should, however, be expected at high temperatures (>850°C) and positive stress ratio, where creep damage coexists with fatigue damage, or even dominates [19, 28].

Performance of TMS-238, CMSX-4 Plus, and TROPEA at LCF Conditions

The difference in LCF life between CMSX-4 Plus, TMS-238, and TROPEA results from a clear difference in the first LCF loops, as shown in Fig. 5a. TMS-238 has a pronounced plastic deformation during the first cycle, while TROPEA and CMSX-4 Plus present almost no plasticity under the same temperature and maximum applied stress of 950 MPa. Although an almost fully elastic loop is obtained since cycle 2 for TMS-238 under this condition, the large plastic deformation at cycle 1 leads to a very pronounced slip localization, overall leading to an earlier crack initiation from pore (see Fig. 3b), serving as notches. At σ_{Max} = 950 MPa, TMS-238 has a LCF life nearly two times smaller than the one obtained for TROPEA and CMSX-4 Plus.

To better understand the LCF durability, and more specifically the contribution of YS to the LCF life, the cyclic behavior of TMS-238, CMSX-4 Plus, and TROPEA was compared at iso-maximum stress with respect to the YS value, i.e., same σ_{Max}/YS ratio, see Fig. 5b. The LCF

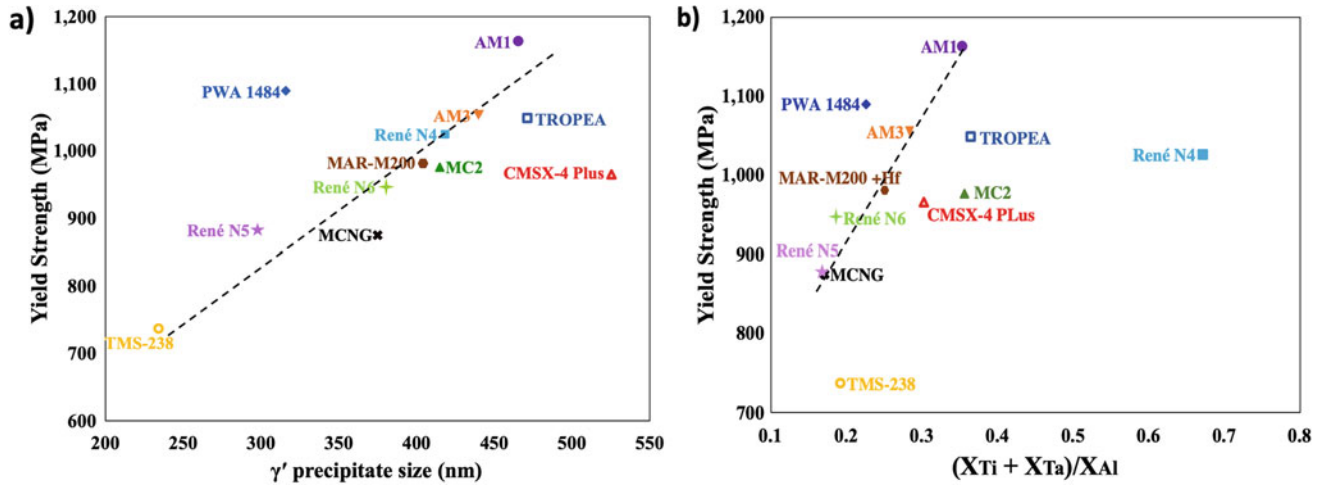

Fig. 6 Yield stress, measured at 0.05 pct. plastic offset, plotted as a function of the γ'-precipitate size (nm) (**a**) and as a function of the $(X_{Ti} + X_{Ta})/X_{Al}$ ratio (X in at. pct.) (**b**). A black dotted main trendline is added in each plot

endurance is almost the same. Moreover, it is observed that TMS-238 stabilizes since cycle 2 while TROPEA and CMSX-4 Plus are reaching elastic loops after at least five cycles. This faster elastic accommodation of TMS-238 is a result of its very steep hardening, see Fig. 4b. The differences in the YS are hence the main criteria controlling the LCF life in this condition.

Influence of Chemical Composition on Tensile Properties at 650 °C

A difference in γ'-precipitate size in primary dendrite arms, and interdendritic region, as well as the channel width has been noticed for TMS-238. The γ'-precipitate average size is around 55% smaller, and the channel width is around 30% smaller than those reported for CMSX-4 Plus. This difference in size is known to impact the mechanical properties of Ni-based superalloys [29]. Sengupta et al. have documented that the YS increases with the increasing of γ'-precipitate size for CMSX-4 at different temperatures, with a peak in the 700–800 °C temperature range [30]. On the contrary, Shah et al. [31] have showed for PWA 1480 that the YS is almost insensitive to the γ'-precipitate size in the same temperature range. However, for temperatures around 650 °C, the YS decreases with the increasing of γ'-precipitates. In the present study, a correlation between the YS (MPa) and the γ'-precipitate size (nm) for all superalloys tested is detailed in Fig. 6a. The results induce the conclusion that the microstructure is the main parameter to control the YS.

Conversely, Caron et al. have proved that the alloy composition strongly influences the YS and the hardening behavior of SX Ni-based superalloys [32]. In the same study, a great care was taken to assess the effect of chemical composition of various SX Ni-based alloys having the same precipitate size and crystalline orientation. They concluded that the YS variation is mainly related to the ratio in the concentrations in atomic percent of Ti + Ta over the concentration of Al, results in Table 4. These elements are well known to be γ' former. They increase the APB energy consequently contributing to the resistance to precipitate shearing. TMS-238 does not contain Ti, which should be replaced in the γ' precipitate by other elements such as Ta (~2.7 at. pct.). The absence/low concentration of Ti/Ta compared to Al influenced the γ' resistance to shearing, decreasing the YS at 650 °C [31–33].

Regarding the results presented in Table 4, the ratio for TMS-238 is around 0.19, while it is of 0.30 for CMSX-4 Plus and 0.37 for TROPEA. It hence seems that the higher the ratio, the higher the YS at 650 °C. A similar conclusion was obtained by Caron et al. [32] at fixed precipitate size. They suggested that the superalloys chemistry, especially the γ' one, is the key to this evolution. Figure 6b also shows that the YS is highly influenced by the superalloys chemistry. It is worth noting that both superalloys outside the main trend in this figure (TMS-238 and René N4) present a strong hardening (see Fig. 4) and low ductility. This may result from a higher density of sub-grain/low angle boundaries at the dendrite/interdendritic interfaces if a very fast cooling rate (greater than 500 °C/min) at the end of the solution heat treatment has been used, leading to pronounced dendritic stresses [34]. If this is the case, a higher density of sub-grain boundaries may trigger earlier yielding, more hardening, and lower ductility due to a lower mean free path for dislocation/slip bands. This assumption remains to be checked objectively.

Among all alloys subjected to tensile test at 650 °C, TMS-238 showed a particular behavior with a very low YS

and a very spectacular work hardening. The specific chemistry and high misfit of the alloy can be the reasons for such an atypical behavior. Compared to other alloys, TMS-238 is estimated to have a ~5% lower fraction of γ' due to its slightly lower content of main γ' forming element (sum of Ti + Ta + Al contents). Although it has a high Ta content, overall Al-substitution element that partitions into γ' phase is lower than other alloys that performed well in the tensile test, such as CMSX-4 Plus, TROPEA, and PWA1484. Ta and Ti are known to increase anti-phase boundary (APB) energy that increases precipitate's resistance to shearing by ½ <110> pair dislocations. Lower strength of γ' phase is the most probable reason of lower YS for TMS-238 [17, 35]. On the other hand, partition of alloying elements, particularly very high Re content in γ phase in TMS-238, decreases stacking fault energy of γ matrix [35]. Activation and interaction of multiple slip systems by APB shearing and interaction of stacking faults in the matrix both may be contributed to this distinctive work hardening. Based on the literature results [33], a possibility to improve fatigue performances of TMS-238 at fixed chemistry would be an increase in the γ' size keeping the regularity in γ' morphology inherited from the very high misfit of the alloy. This can only be achieved by using slower cooling rates and/or longer/hotter aging HTs [36], without affecting the coherency of the precipitates with the matrix.

TROPEA Chemistry and Its Mechanical Performance

TROPEA has the precious metal element Pt in its composition. It is known to stabilize the γ' precipitate and to increase its solvus temperature [13, 17]. This new scenario with a γ' composition of $(Ni, Pt)_3(Al, Ta, Ti)$ seems to be beneficial to the tensile properties of TROPEA. Indeed, according to Table 4, TROPEA holds the best compromise in terms of YS/elongation at failure. This very high YS and strain at failure have been obtained with all the room temperature, i.e., 850 °C temperature range.

Even though TROPEA presents ~13% of eutectics due to its high Ta content and the introduction of Pt, overall closing the solution HT window, the presence of such metallurgical defects has no detrimental impact on the LCF properties of the material. This result is in fact in good agreement with a previous comprehensive study on the role of metallurgical defects such as pores, γ/γ' eutectics pools, incipient melting, and chemical homogeneity across the dendritic structure on the fatigue life variability of CMSX-4 Plus [11]. Further information about TROPEA's chemical development and creep properties is detailed in Rame et al. [9].

While the cost of TROPEA and TMS-238 is comparable, TROPEA has shown a good compromise between the YS, elongation at failure, and more importantly, a very good performance in LCF at low temperatures. However, the exact role of Pt remains to be understood, especially in terms of YS and how its partitioning coefficient evolves as a function of temperature. TROPEA alloy, in itself, is a very first trial to investigate how minor additions of Pt in the chemical composition could impact mechanical properties. Still, the present results are showing potential of Pt bearing SX Ni-based superalloy that exhibits very good tensile behavior for turbine blade material, with an acceptable density [9].

Conclusions

Tensile and LCF at 650 °C, and VHCF at 1000 °C have been investigated for three main SX Ni-based superalloys: CMSX-4 Plus (3rd generation alloy and chosen as a reference), TMS-238 (6th generation alloy), and TROPEA (a newly developed Pt-containing alloy). The influence of chemistry on tensile properties was investigated adding nine other SX Ni-based superalloys to the analysis. The following main conclusions have been obtained:

- The solidification parameters and consequently the casting pore size are still the main parameters controlling the VHCF life at 1000 °C/20 kHz/R_ε = -1.
- The yield stress is directly affected by the chemical composition of the SX Ni-based superalloys. Ti and Ta are very effective elements to increase the resistance of γ' precipitates to shearing.
- The yield stress is the main parameter controlling the low cycle fatigue (at 650 °C, R_σ = 0.05/f = 0.5 Hz) life.
- Despite having a low yield stress, TMS-238 presents a remarkable strain hardening, overall leading to a fast cyclic stabilization in LCF at 650 °C.
- TROPEA alloy has superior fatigue endurance in LCF at 650 °C compared to CMSX-4 Plus and TMS-238 alloys due to its higher yield stress, mainly resulting from its high Ta content.
- LCF and VHCF properties do not seem to be impacted directly by the presence of Pt in the chemical composition.

Acknowledgments SAFRAN Tech/PFX is gratefully acknowledged for providing CMSX-4 Plus and TROPEA SX bars. NIMS is gratefully acknowledged for providing TMS-238 SX bars, especially Dr. Toshiharu Kobayashi, Dr. Tadaharu Yokokawa, and Mr. Yuji Takata. LMBO, SU, and JC gratefully acknowledge Dr. Pierre Caron (formerly

at ONERA) for fruitful discussions. Likewise, they wish to thank Mrs. Florence Hamon, Mr. Florent Mauget, and Mr. Jacques Lefort (Physics and Mechanics of Materials Department, Institut Pprime, France) for their help and advices during mechanical testing and microstructural observations.

References

1. (2019) Statista. In: Annu. growth Glob. air traffic Passeng. demand from 2006 to 2019. https://www.statista.com/statistics/193533/growth-of-global-air-traffic-passenger-demand/. Accessed 9 Jul 2019
2. Reed RC (2005) The superalloys: fundamentals and applications. 363
3. Pollock TM, Tin S (2008) Nickel-Based Superalloys for Advanced Turbine Engines: Chemistry, Microstructure and Properties. J Propuls Power 22:361–374. https://doi.org/10.2514/1.18239
4. Caron P (2000) High gamma prime solvus new generation Nickel-based superalloys for single crystal turbine blade applications. Superalloys 2000 737–746. https://doi.org/10.7449/2000/Superalloys_2000_737_746
5. Zhang WJ (2016) Thermal mechanical fatigue of single crystal superalloys: Achievements and challenges. Mater Sci Eng A 650:389–395. https://doi.org/10.1016/j.msea.2015.10.078
6. Wahl JB, Harris K (2016) CMSX-4 Plus Single Crystal Alloy Development, Characterization and Application Development. Superalloys 2016 25–33. https://doi.org/10.1002/9781119075646.ch3
7. Kawagishi K, Yeh AC, Yokokawa T, et al (2012) Development of an Oxidation-Resistant High-Strength Sixth-Generation Single-Crystal Superalloy TMS-238. Superalloys 2012 189–195. https://doi.org/10.1002/9781118516430.ch21
8. Rame J, Cormier J (2019) Ni-based superalloy for single crystalline turbine French Patent. (A1)
9. Rame J, Utada S, Bortoluci Ormastroni LM, et al (2020) Platinum containing new generation nickel-based superalloys for single crystalline applications. Superalloys 2020
10. Harris K, Wahl JB (2016) High strength single crystal superalloy. US Patent. US9518311B2. https://patents.google.com/patent/US9518311B2/en
11. Bortoluci Ormastroni LM, Mataveli Suave L, Cervellon A, et al (2020) LCF, HCF and VHCF life sensitivity to solution heat treatment of a third-generation Ni-based single crystal superalloy. Int J Fatigue 130. https://doi.org/10.1016/j.ijfatigue.2019.105247
12. Cormier J (2016) Thermal Cycling Creep Resistance of Ni-Based Single Crystal Superalloys. Superalloys 385–394
13. Tin S, Zhang L, Ofori AP, Miller MK (2007) Atomic partitioning of platinum and ruthenium in advanced single crystal Ni-based superalloys. Mater Sci Forum 546–549:1187–1194. https://doi.org/10.4028/www.scientific.net/msf.546-549.1187
14. Corti CW, Coupland DR, Selman GL (1980) Platinum-Enriched Superalloys. Platin Met Rev 2–11
15. Chen Y, Zhao X, Bai M, et al (2015) Effect of platinum addition on oxidation behaviour of γ/γ′ nickel aluminide. Acta Mater 86:319–330. https://doi.org/10.1016/j.actamat.2014.12.023
16. Gleeson B, Wang W, Hayashi S, Sordelet D (2004) Effects of platinum on the interdiffusion and oxidation behavior of Ni-Al-based alloys. Mater Sci Forum 213–222. https://doi.org/10.4028/www.scientific.net/msf.461-464.213
17. Vattré A, Devincre B, Roos A (2009) Dislocation dynamics simulations of precipitation hardening in Ni-based superalloys with high γ′ volume fraction. Intermetallics 17:988–994. https://doi.org/10.1016/j.intermet.2009.04.007
18. Van Sluytman JS (2010) Microstructure and High Temperature Creep of Platinum Group Metal Modified Nickel Base Superalloys. University of Michigan. https://deepblue.lib.umich.edu/handle/2027.42/77722
19. Cervellon A (2018) Propriétés en fatigue à grand et très grand nombre de cycles et à haute température des superalliages base nickel monogranulaires. PhD Thesis - Ecole Nationale Superieure de Mecanique et D'Aerotechnique. http://theses.fr/2018ESMA0009
20. Cervellon A, Cormier J, Mauget F, et al (2018) Very high cycle fatigue of Ni-based single crystal superalloys at high temperature. Metall Mater Trans A 49:3938–3950. https://doi.org/10.1007/s11661-018-4672-6
21. Cervellon A, Cormier J, Mauget F, Hervier Z (2017) VHCF life evolution after microstructure degradation of a Ni-based single crystal superalloy. Int J Fatigue 104:251–262. https://doi.org/10.1016/j.ijfatigue.2017.07.021
22. Cervellon A, Hemery S, Kürnsteiner P, et al (2020) Crack initiation mechanism during very high cycle fatigue of Ni-based single crystal superalloys at high temperature. Acta Mater 188:131–144. https://doi.org/10.1016/j.actamat.2020.02.012
23. Vaunois J-R, Cormier J, Villechaise P, et al (2010) Influence of both γ' distribution and grain size on the tensile properties of UDIMET 720Li at room temperature. Superalloy 718 199–213
24. Karunaratne MS., Carter P, Reed R. (2000) Interdiffusion in the face-centred cubic phase of the Ni–Re, Ni–Ta and Ni–W systems between 900 and 1300°C. Mater Sci Eng A 281:229–233. https://doi.org/10.1016/S0921-5093(99)00705-4
25. Steuer S, Villechaise P, Pollock TM, Cormier J (2015) Benefits of high gradient solidification for creep and low cycle fatigue of AM1 single crystal superalloy. Mater Sci Eng A 645:109–115. https://doi.org/10.1016/j.msea.2015.07.045
26. Diologent F (2002) Comportement en fluage et en traction de superalliages monocristallins à base de nickel. PhD Thesis - Universite Paris XI UFR Scientifique d'Orsay. http://theses.fr/2002PA112300
27. Mataveli Suave L (2017) High temperature durbaility of DS200 + Hf alloy. PhD Thesis - École Nationale Superieure de Mecanique et d'Aerotechnique
28. Cervellon A, Yi JZ, Corpace F, et al (2020) Creep, fatigue, and oxidation interactions during High and very high cycle fatigue at elevated temperature of nickel-base single crystal superalloys. Superalloys 2020
29. Long H, Mao S, Liu Y, et al (2018) Microstructural and compositional design of Ni-based single crystalline superalloys—A review. J Alloys Compd 743:203–220. https://doi.org/10.1016/j.jallcom.2018.01.224
30. Sengupta A, Putatunda SK, Bartosiewicz L, et al (1994) Tensile behavior of a new single crystal nickel-based superalloy (CMSX-4) at room and elevated temperatures. J Mater Eng Perform 3:664–672. https://doi.org/10.1007/BF02645265
31. Shah DM, Duhl DN (2012) The Effect of Orientation, Temperature and Gamma Prime Size on the Yield Strength of a Single Crystal Nickel Base Superalloy. 105–114. https://doi.org/10.7449/1984/superalloys_1984_105_114
32. Caron P, Diologent F, Drawin S (2011) Influence of chemistry on the tensile yield strength of nickel-based single crystal superalloys. Adv Mater Res 278:345–350. https://doi.org/10.4028/www.scientific.net/AMR.278.345
33. Wang-Koh YM (2017) Understanding the yield behaviour of L12-ordered alloys. Mater Sci Technol (United Kingdom) 33:934–943. https://doi.org/10.1080/02670836.2016.1215961
34. Epishin A, Link T, Brückner U, et al (2004) Effects of segregation in Nickel-base superalloys: dendritic stresses. Int Symp Superalloys 537–543. https://doi.org/10.7449/2004/Superalloys_2004_537_543

35. Yuan Y, Kawagishi K, Koizumi Y, et al (2014) Creep deformation of a sixth generation Ni-base single crystal superalloy at 800 °C. Mater Sci Eng A 608:95–100. https://doi.org/10.1016/j.msea.2014.04.069

36. Steuer S, Hervier Z, Thabart S, et al (2014) Creep behavior under isothermal and non-isothermal conditions of AM3 single crystal superalloy for different solutioning cooling rates. Mater Sci Eng A 601:145–152. https://doi.org/10.1016/j.msea.2014.02.046